

Agentic Aerial Cinematography: From Dialogue Cues to Cinematic Trajectories

Yifan Lin^{†*1}, Sophie Ziyu Liu^{*1}, Ran Qi^{*1}, George Z. Xue^{*1}, Xinping Song¹, Chao Qin² and Hugh H.-T. Liu²
<https://acdc-drone.github.io>

Abstract— We present **Agentic Aerial Cinematography: From Dialogue Cues to Cinematic Trajectories (ACDC)**, an autonomous drone cinematography system driven by natural language communication between human directors and drones. The main limitation of previous drone cinematography workflows is that they require manual selection of waypoints and view angles based on predefined human intent, which is labor-intensive and yields inconsistent performance. In this paper, we propose employing large language models (LLMs) and vision foundation models (VFMs) to convert free-form natural language prompts directly into executable indoor UAV video tours. Specifically, our method comprises a vision-language retrieval pipeline for initial waypoint selection, a preference-based Bayesian optimization framework that refines poses using aesthetic feedback, and a motion planner that generates safe quadrotor trajectories. We validate ACDC through both simulation and hardware-in-the-loop experiments, demonstrating that it robustly produces professional-quality footage across diverse indoor scenes without requiring expertise in robotics or cinematography. These results highlight the potential of embodied AI agents to close the loop from open-vocabulary dialogue to real-world autonomous aerial cinematography.

Index Terms— AI-Enabled Robotics, Aerial Systems: Perception and Autonomy, Semantic Scene Understanding

I. INTRODUCTION

Unmanned aerial vehicles (UAV) are widely used in cinematography, yet human pilots remain heavily in the loop and overall automation is limited [1]–[3]. One key reason is that natural language lacks precision and often contains significant ambiguity, making it challenging to paraphrase into language that robots can understand and execute. For example, people might express their needs with sentences like, “Shoot a video that shows how spacious this house feels.” While this intent can be interpreted by humans with ease, no prior method can transform it into accurate trajectory for the UAVs to follow in order to obtain the desired footage without crashes. To unlock the next level of automation, it is of great value to accomplish the autonomous drone cinematography task shown in Fig. 1, where a human can communicate with the drone using open-vocabulary natural language and obtain the desired video with satisfactory details.

Recent advances in Large Language Models (LLMs) and Vision Foundation Models (VFMs) enable robots to interpret natural language, allowing non-experts to express

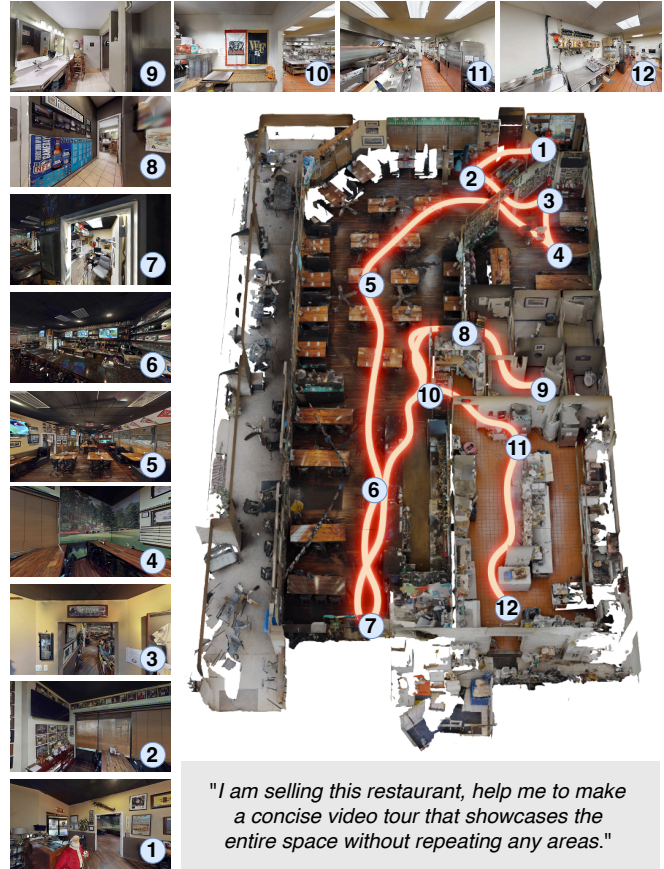


Fig. 1. In this paper, we introduce the Autonomous Drone Cinematography (ACDC) task. Given a natural-language instruction, ACDC generates a video by planning a sequence of drone waypoints. The figure shows an example: starting from a vague instruction, ACDC produces a flight path with 12 ordered waypoints (labeled 1–12).

goals without explicit programming [4]–[6]. However, these models have limited spatial awareness and have trouble understanding the physical robot constraints. As a result, they cannot reliably generate trajectories that both meet the intent and remain dynamically feasible and collision-free [7], [8]. To our knowledge, no prior work has demonstrated natural-language-level collaboration with autonomous UAVs that closes the loop from open-ended prompts to professional-quality footage in constrained indoor environments.

In this paper, we present **Agentic aerial Cinematography: From Dialogue cues to Cinematic trajectories (ACDC)** to enable fully autonomous drone cinematography. The in-

arXiv:2509.16176v1 [cs.RO] 19 Sep 2025

[†]Project lead, ^{*}Equal contribution (alphabetical order)

¹Division of Engineering Science, University of Toronto

²Institute for Aerospace Studies, University of Toronto

Corresponding authors: Yifan Lin i.lin@mail.utoronto.ca, Hugh H.-T. Liu hugh.liu@utoronto.ca

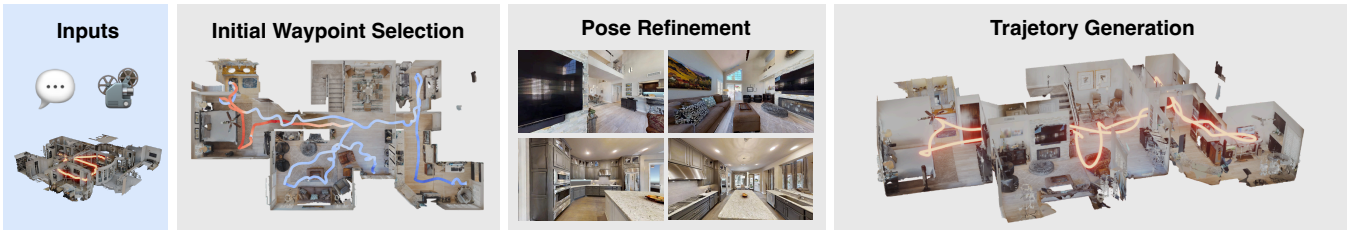


Fig. 2. **System overview of ACDC.** Given a natural-language prompt, an exploratory video, and a photorealistic 3D reconstruction, ACDC (i) retrieves and orders initial waypoints via vision–language similarity (Sec. III-A), (ii) refines each pose with preference-based Bayesian optimization (Sec. III-B), and (iii) generates a smooth, collision-free, dynamically feasible quadrotor trajectory for execution (Sec. III-C).

puts to the system include an exploratory video, a high-fidelity 3D environment model, and a free-form prompt. In the first step, we employ vision–language retrieval and frame–language similarity to select keyframes or candidate viewpoints, similar to [9], [10]. Then, a preference-based Bayesian optimization (BO) process is performed over pose, treating the natural-language prompt as the optimization objective through language and aesthetic feedback [11]–[13]. Subsequently, our method plans a smooth, collision-free, dynamical-feasible trajectory passing through the refined waypoints in the specified order. Finally, the trajectory is executed by an onboard controller to acquire the target footage. See Fig. 2 for an illustration of the overall system. We demonstrate that ACDC enables users with no robotics or cinematography expertise to obtain professional-grade indoor footage. Our contributions are summarized below:

- To the best of our knowledge, ACDC is the first system to turn free-form, abstract natural language input directly into executable indoor UAV video tours.
- We proposed a language-conditioned Bayesian optimization scheme, which refines visibility-oriented initial camera poses to meet aesthetic goals.
- We performed simulation and hardware-in-the-loop experimentation to demonstrate the quality and robustness of the proposed system.

II. RELATED WORK

A. Autonomous Drone Cinematography

Before the recent advances in LLMs, most research on autonomous drone cinematography focuses on designing optimization-based UAV planners [1], [3], [14]–[16], with deep learning used in limited cases [17], [18]. However, these works largely rely on fixed shot grammars or hand-tuned objectives and discrete shot modes rather than free-form natural language, and they fall short of providing a fully end-to-end pipeline that enables users with no cinematography or technical expertise to generate professional-quality videos directly from intent.

Since the rise of VLMs, recent works have explored integrating pretrained semantic models into cinematography, including natural-language guided photography [19], conversational camera control [20], and multi-agent systems for end-to-end virtual filmmaking [21]. However, to our

knowledge, none have developed a complete pipeline for a robust embodied AI agent capable of drone cinematography.

B. Embodied AI Agents

With the advent of large foundational models, embodied AI agents in robotics have advanced rapidly. General systems such as SayCan, PaLM-E, LM-Nav, and Swarm-GPT demonstrate language-grounded control on real robots across manipulation, navigation, and multi-robot choreography [4]–[6], [22]. In the UAV domain, FM-Planner and LEVIOSA convert natural-language instructions into obstacle-aware navigation trajectories; by contrast, they do not address cinematographic objectives [7], [8].

C. Application of VFMs and LLMs

With the rise of CLIP-style contrastive vision–language models [23]–[25], recent work has explored their large-scale use in video and robotics. KeyVideoLLM [26] proposed keyframe selection directly via frame–language similarity, a concept closely aligned with our approach. Other methods extend contrastive embeddings to query-aware video selection [10], place recognition and retrieval [27], [28], embodied AI navigation [29], [30], and beyond. These works demonstrate the effectiveness of contrastive embeddings for aligning visual data with language, which we employ in the context of cinematic drone trajectory generation in this paper.

D. Preference-Based Bayesian Optimization

Preference-based Bayesian optimization (PBO) has solid theoretical foundations in GP preference learning with a Bradley–Terry likelihood, and has been adapted from early interactive graphics/design to modern visual appearance optimization and constrained creative design. [11]–[13], [31], [32]. Test-time canonicalization/adaptation improves robustness by aligning inputs at inference: e.g., FOCAL leverages foundation-model priors for test-time canonicalization of visual inputs, and Pose-TTA aligns head pose at test-time for pose-invariant recognition; both are directly applicable to stabilizing pairwise visual comparisons. [33], [34]. Language-supervised view selection has been studied in multi-view video: *Which Viewpoint Shows it Best? (LangView)* [35] uses accompanying language to weakly supervise ‘best-view’ selection and learns a selector that generalizes at inference without language/camera poses. Together, these

directions—PBO under BT-GP models, test-time canonicalization, and language-supervised view selection—provide complementary tools for robust, sample-efficient preference learning on visual inputs; our method instantiates this with BT-GP modeling and a dueling-bandit acquisition [11], [12].

III. METHODOLOGY

The task of autonomous drone cinematography requires two primary inputs:

- **Exploratory scan:** a user-recorded indoor exploration video $\mathcal{V} = \{I_t\}_{t=1}^T$ that scans the environment in a coverage-oriented, non-aesthetic manner. The scan is intended to be used to create in a 3D reconstruction of the environment using methods such as Gaussian Splatting in real-world deployment.
- **Prompt:** a description in natural language \mathcal{P} of the desired cinematic shot(s).

And three auxiliary inputs:

- **Pose of each initial frame:** $\{\mathbf{T}_t\}_{t=1}^T$, $\mathbf{T}_t \in \text{SE}(3)$, obtained by running a localization algorithm from LIDAR and IMU rigidly attached to the camera.
- **Traversability map:** Voxel-based traversability map \mathcal{M} obtained from processing localization result and LIDAR reading.
- **Photorealistic 3D reconstruction:** a scene representation \mathcal{S} reconstructed from \mathcal{V} (e.g., 3D Gaussian Splatting or a textured mesh) used for rendering in Sec. III-B.

The final output is a discretized series of controls $\mathcal{U} = \{\mathbf{u}_{1:N}\}$ for the drone.

Given these inputs and output, ACDC operates in three stages. First, *Initial Waypoint Selection* retrieves candidate frames from the exploratory scan that are semantically aligned with the prompt, prunes and orders them into an initial waypoint sequence that reflects user intent. Second, *Pose Refinement* adjusts each waypoint’s position and orientation to yield views that are more aesthetic and better aligned with the prompt. Finally, *Trajectory Generation* synthesizes a smooth, dynamically feasible, collision-free flight that passes through the refined waypoints.

A. Initial Waypoint Selection

Given a prompt and a video sequence capable of creating a 3D reconstruction of the scene, an intuitive yet naive solution would be to design an agent that can freely explore the reconstructed environment, capture images, and interface with VLM. However, images captured from 3D reconstruction renderings often have lower quality compared to photos taken in the real world, and limit VLM’s ability to understand the scene.

To address this challenge, we opt for directly using the exploration video as input and employ a vision–language retrieval pipeline that can efficiently extract an ordered sequence of key frames with their corresponding poses that reflect both the prompt content and the intended temporal flow of the shot. As shown in Fig. 3, the pipeline consists of the following steps:

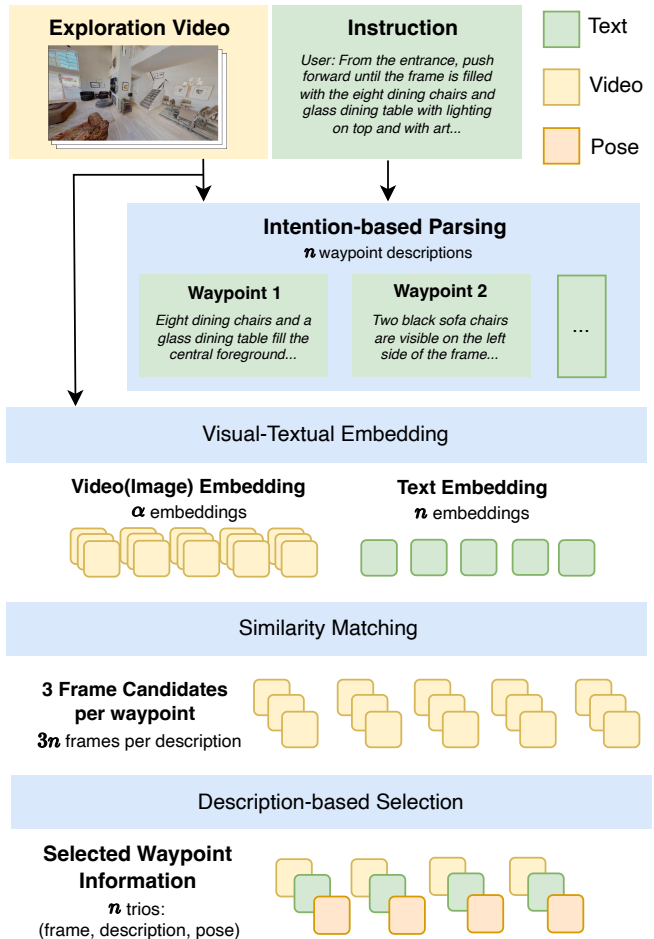


Fig. 3. In section III-A, we introduce a waypoint selection algorithm, where a user-provided exploration video and instruction are processed. First, the exploration video and instructions are processed by a large language model into n waypoint descriptions. These descriptions are then converted into embeddings by a vision foundation model. Finally, the large language model selects n waypoint trios.

1) *Waypoint Description Generation:* Given the exploration video, an VLM summarizes it into an environment description \mathcal{E} and, conditioned on $(\mathcal{P}, \mathcal{E})$, generates n waypoint descriptions $\{\mathcal{D}_k\}_{k=1}^n$.

2) *Input Encoding:* A pretrained VFM encodes each description as $\mathbf{d}_k = \phi_{\text{txt}}(\mathcal{D}_k)$ and each frame I_t as $\mathbf{i}_t = \phi_{\text{img}}(I_t)$ using the same model.

3) *Candidate Retrieval:* For each \mathbf{d}_k , compute cosine similarities between it and all \mathbf{i}_t . Select three top-matching frames, forming a candidate set C_k .

4) *Select and Sort:* A multi-modal VLM is queried with $\{\mathcal{D}_k\}_{k=1}^n$ and frames in $\{C_k\}_{k=1}^n$ to choose the best-matching frame for each waypoint and to order waypoints according to the user-intended flow.

The result of this stage is an ordered set of initial posed-waypoints

$$\check{\mathcal{T}} = \{\mathbf{T}_0, \mathbf{T}_1, \dots, \mathbf{T}_{j,0}\} \subset \{C_k\}_{k=1}^n,$$

These waypoints form the starting trajectory skeleton and

are subsequently refined by the preference-based Bayesian optimization stage.

B. Pose Refinement

The waypoints produced by the select-and-sort stage are constrained to poses that appear in the exploratory video. As a result, their viewpoints are inherently limited by how the video was captured, both in position and in viewing angle. Since these initial waypoints are usually relatively close to the target, we now provide ACDC with full access to the 3D reconstructed scene. Allowing it to move freely in space and dial in the perfect shot. The role of the refinement stage is to optimize a semantically aligned but potentially suboptimal waypoint by locally searching the pose space for a view that better satisfies the prompt while remaining feasible. While the refinement pipeline supports full 6-DoF optimization—translation \mathbf{p} and rotation $\mathbf{q} \in \text{SO}(3)$ —in our aerial-filming setting we restrict rotation to the one-parameter subgroup about the world z -axis. Accordingly, we optimize in the 4-DoF space $[\mathbf{p}, \theta]$ with $\theta \in S^1$ and instantiate the rotation as $\mathbf{q} = \mathbf{q}_z(\theta)$. Rotations about the remaining axes are held fixed to be 0. This restriction reduces the search space while preserving feasibility and composition objectives.

Algorithm 1 Pose Refinement via Preference-Based Bayesian Optimization on 6-DoF pose $[\mathbf{p}, \mathbf{q}]$

Require: Candidate poses and descriptions $\{(\mathbf{T}_i, d_i)\}_{i=1}^n$; scene \mathcal{S} ; VLM scorer Φ ; iterations B ; candidates per iteration M ; trust-region radii $(\rho_{\text{rot}}, \rho_{\text{trans}})$

- 1: Initialize GP $f \sim \mathcal{GP}(0, k)$ on $S^1 \times \mathbb{R}^3$
- 2: **for** $i = 1$ to n **do**
- 3: $\hat{\mathbf{T}} \leftarrow \mathbf{T}_i$ ▷ Represent best pose
- 4: **for** $t = 1$ to B **do**
- 5: $X_t \leftarrow \text{SAMPLECANDIDATES}(\hat{\mathbf{T}}, M, \rho_{\text{rot}}, \rho_{\text{trans}})$
- 6: $a_{1:M} \leftarrow A(\hat{\mathbf{T}}, X_t, f)$ ▷ per-candidate advantages
- 7: $m^* \leftarrow \arg \max_{m \in \{1, \dots, M\}} a_m$
- 8: $\mathcal{S}_t \leftarrow \text{COLLECTPREFERENCES}(\Phi, \hat{\mathbf{T}}, x_{m^*})$ ▷ VLM comparison
- 9: $f \leftarrow \text{UPDATEPOSTERIOR}(f, \mathcal{S}_t)$
- 10: **if** $\text{PREFERS}(x_{m^*}, \hat{\mathbf{T}} \mid \mathcal{S}_t)$ **then**
- 11: $\hat{\mathbf{T}} \leftarrow x_{m^*}$
- 12: **end if**
- 13: **end for**
- 14: $\mathbf{T}_{i,\text{ref}} \leftarrow \hat{\mathbf{T}}$
- 15: **end for**
- 16: **return** $\mathcal{T}_{\text{ref}} \leftarrow \{\mathbf{T}_{i,\text{ref}}\}_{i=1}^n$

While the refinement module can optimize full 6-DoF poses—translation \mathbf{p} and rotational \mathbf{q} —in our aerial-filming setting we restrict rotation to the one-parameter subgroup about the vertical axis.

The refinement pipeline is capable of optimizing over \mathbf{p} and \mathbf{q} , however, in the practice of optimizing over drone shots, we choose to only optimize for yaw and set pitch and roll to practically zero. \mathbf{q} will be used to represent yaw only.

We take as input a set of candidate poses $\mathcal{C} = \{\mathbf{T}_i\}_{i=1}^N$ extracted from the exploratory video, where each pose \mathbf{T}_i is paired with a concise textual description \mathbf{d}_i summarizing what that viewpoint is intended to capture. These candidates serve as seeds for downstream selection and refinement rather than final shots. In addition, we assume access to a reconstructed 3D scene \mathcal{S} that acts as a geometric and photometric proxy for both rendering and collision checking. In deployment, \mathcal{S} is produced with *Gaussian Splatting*; in our experiments we approximate \mathcal{S} with a LiDAR-based reconstruction that fulfills the same role. All poses \mathbf{T}_i and the scene \mathcal{S} are expressed in a consistent world frame so that we can synthesize views at candidate poses and verify feasibility (e.g., obstacle clearance) using the same representation.

We treat refinement as a preference-based Bayesian optimization loop, where the goal is to learn which nearby pose produces the most aesthetic view.

1) *GP Prior:* We assume each pose \mathbf{T} has an unknown “aesthetic utility” $f(\mathbf{T})$. To model $f(\cdot)$ smoothly, we place a Gaussian Process (GP) prior $f \sim \mathcal{GP}(0, k)$ and use a covariance that factorizes over rotation and translation.

$$k(\mathbf{T}_i, \mathbf{T}_j) = k_{\text{rot}}(\mathbf{q}_i, \mathbf{q}_j) k_{\text{trans}}(\mathbf{p}_i, \mathbf{p}_j) + \varepsilon \delta_{ij},$$

Here k_{rot} measures similarity via the $\text{SO}(3)$ geodesic between unit quaternions \mathbf{q}_i and \mathbf{q}_j while k_{trans} is a squared-exponential kernel on the Euclidean distance between positions \mathbf{p}_i and \mathbf{p}_j . Algorithm 1 initializes this prior once and then refines each seed locally.

2) *Choosing the Next Pose:* We sample $M = 64$ new pose candidates each iteration. Let the current incumbent be $\hat{\mathbf{T}} = [\mathbf{p}_{\text{best}}, \theta_{\text{best}}]$ with trust-region radii $(\rho_{\text{rot}}, \rho_{\text{trans}})$. For $m = 1, \dots, 64$:

$$\begin{aligned} \text{(rotational)} \quad & \Delta\theta_m \sim \text{Unif}[-\rho_{\text{rot}}, \rho_{\text{rot}}], \\ & \theta_m = \text{wrap}(\theta_{\text{best}} + \Delta\theta_m), \\ & \mathbf{q}_m = \theta_m; \end{aligned}$$

$$\begin{aligned} \text{(translational)} \quad & u_m \sim \text{Unif}(S^2) \\ & r_m \sim \text{Unif}[0, \rho_{\text{trans}}], \\ & \delta\mathbf{p}_m = r_m u_m, \\ & \mathbf{p}_m = \text{clamp}_{\text{JefT}}(\mathbf{p}_{\text{best}} + \delta\mathbf{p}_m); \end{aligned}$$

$$\text{(candidate)} \quad x_m = (\mathbf{p}_m, \mathbf{q}_m)$$

As outlined in Algorithm 1, we select a challenger x_m^* using Dueling Thompson Sampling.

$$\begin{aligned} \tilde{f} & \sim \mathcal{N}(\mu, \Sigma) \quad (\text{posterior over } \{\hat{\mathbf{T}}\} \cup X_t), \\ a_m & = \tilde{f}(x_m) - \tilde{f}(\hat{\mathbf{T}}), \quad m = 1, \dots, M, \\ m^* & = \arg \max_m a_m, \quad \text{challenger} = x_{m^*}. \end{aligned}$$

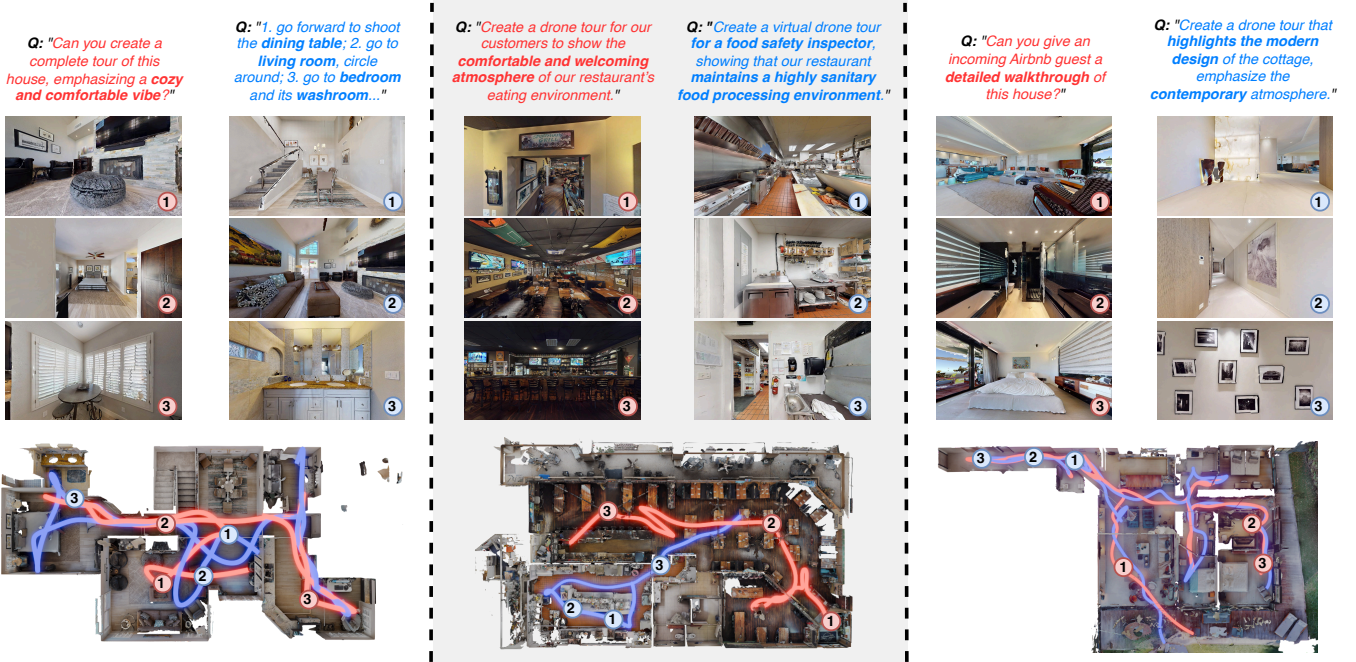


Fig. 4. **Qualitative rollouts across three scenes.** Columns correspond to simulated scenes—(left) *cottage*, (middle) *restaurant*, (right) *luxury*. For each scene, we show two ACDC trajectories generated from the prompt shown above; three representative keyframes per trajectory are displayed, and the pair of path overlays for the scene appears at the bottom.

3) *Preference Feedback*: We render the incumbent \hat{T} and a challenger x_{m^*} , present the two views with the instruction to a vision–language model, and record a single binary comparison s_{ij} . In Algorithm 1 this label is stored in the per-iteration comparison set S_t . The comparison is encoded with the Bradley–Terry likelihood

$$p(s_{ij} | f_i, f_j) = \sigma(s_{ij} (f_i - f_j)), \quad s_{ij} \in \{+1, -1\},$$

which links the probability of choosing one view to the latent utility difference.

4) *Update Posterior*: Each new comparison updates the GP, giving us a posterior distribution over $f(\mathbf{T})$ indicating current best estimate over “aesthetic utility” scores over regions.

Iteratively, this loop steadily improves the estimate of $f(\mathbf{T})$ and converges to a refined pose that better aligns with the user’s intent.

The refinement stage produces a set of n refined poses:

$$\mathcal{T}_{\text{ref}} = \{\mathbf{T}_{k,\text{ref}}\}_{k=1}^n$$

that provide improved framing for the user’s prompt.

C. Trajectory Generation

Given refined waypoints $\mathcal{T}_{\text{ref}} = \{\mathbf{T}_{k,\text{ref}}\}_{k=1}^n$ with positions $\mathbf{p}_{k,\text{ref}}$ and yaw $\theta_{k,\text{ref}}$, and a voxel traversability map \mathcal{M} , we produce a time-parameterized, collision-free trajectory in three concise steps.

1) *Path Extraction*: We connect the waypoint positions in order using A* on the free-voxel graph of \mathcal{M} , yielding a collision-free polyline

$$\mathcal{P} = \{\mathbf{c}_\ell\}_{\ell=1}^L, \quad \mathbf{c}_1 = \mathbf{p}_{1,\text{ref}}, \quad \mathbf{c}_L = \mathbf{p}_{n,\text{ref}},$$

that visits every $\mathbf{p}_{k,\text{ref}}$ sequentially.

2) *Rectangular-Tunnel Corridor*: For each segment $(\mathbf{c}_\ell, \mathbf{c}_{\ell+1})$, let \mathbf{t}_ℓ be the unit tangent, choose orthonormal $(\mathbf{n}_\ell, \mathbf{b}_\ell)$ spanning the orthogonal plane, and set $\Delta_\ell = \|\mathbf{c}_{\ell+1} - \mathbf{c}_\ell\|$. We grow a rectangle centered on the segment (leaving margin δ_{safe} via a distance transform) to obtain cross-section (w_ℓ, h_ℓ) . The box \mathcal{B}_ℓ is the set of points whose local coordinates (x_n, x_b, x_t) in the frame $(\mathbf{n}_\ell, \mathbf{b}_\ell, \mathbf{t}_\ell)$ satisfy

$$|x_n| \leq \frac{w_\ell}{2}, \quad |x_b| \leq \frac{h_\ell}{2}, \quad |x_t| \leq \frac{\Delta_\ell}{2}.$$

The corridor is $\mathcal{C} = \{\mathcal{B}_\ell\}_{\ell=1}^{L-1}$; any curve that stays inside \mathcal{C} is collision-free.

3) *Time-Optimal Trajectory Planning*: Treat each \mathcal{B}_ℓ as an oriented gate and use the Time-Optimal Gate-Traversing (TOGT) planner [36] to compute a continuous, piecewise-polynomial position trajectory that *remains* inside \mathcal{C} , *visits* all waypoints, and *respects* quadrotor dynamic limits. Since TOGT does not constrain yaw, let $\{\tau_k\}$ be the times at which $\mathbf{p}(t)$ passes the refined waypoints. Unwrap $\{\theta_{k,\text{ref}}\}$ and fit a C^2 cubic spline $\theta(t)$ through $\{(\tau_k, \theta_{k,\text{ref}})\}$, which results in a trajectory with smooth pans.

IV. EXPERIMENT

We intend to investigate the following questions through our experimentation:

- **Language-to-shot quality.** Does ACDC translate natural-language prompts—ranging from high-level intent to concrete camera directives—into cinematically pleasing, prompt-aligned shots?
- **Cross-scene generalization.** Can ACDC be generalized across a variety of scenes with drastically different visual features?
- **Real-world executability.** Are ACDC-generated trajectories safe and dynamically feasible to execute on physical platforms, while remaining faithful to the planned camera motion?

A. Implementation Details

In both initial waypoint selection (Sec. III-A) and pose refinement (Sec. III-B), we use Gemini 2.5 Pro [37] as the vision–language model and AM-RADIO [38] with a SigLIP 2 adaptor [39] as the pretrained visual encoder. During refinement, each waypoint is optimized for 100 iterations within a trust region of 1m (translation) and 30° (yaw).

ACDC trajectories are executed on hardware using an autopilot stack with a nonlinear Model Predictive Contouring Controller (MPCC). The controller robustly tracks aggressive, yaw-coupled motions; our yaw-aware planning in trajectory generation yields dynamically feasible paths that MPCC executes with low tracking error.

We construct a photorealistic simulator from a selection of indoor scenes from the HM3D dataset [40] and used Unity as our rendering engine. To obtain authentic exploration video as if the user is actually capturing a video for 3D reconstruction in the real world, we constructed a makeshift Virtual Reality (VR) setup utilizing a motion capture system that can actively track the pose of a handheld device mimicking a camera. The handheld device will display the rendered camera image in the simulator given the pose in real time. Because the mocap volume is limited to $6 \times 6 \times 2.5\text{m}$, we introduce a navigation mixer: x-y translation is commanded via a joystick, while z and orientation are taken from mocap, enabling natural exploration of scenes larger than the tracking volume.

B. Qualitative Results

We present six ACDC rollouts across three distinct scenes (Fig. 4). Prompts span (i) fine-grained instruction following, (ii) situation-aware reasoning, and (iii) abstract vibe-level intent. In the second row of the cottage example, ACDC follows step-by-step instructions with unambiguous referential cues. For situation-conditioned prompts, it targets task-relevant subspaces: in the restaurant, it tours the dining area for a “customer” request and prioritizes the kitchen for a “food inspector.” Under vibe-level prompts (e.g., the second luxury example), overall path coverage is similar to a full tour, but at the shot level ACDC selects characteristic viewpoints and keyframes that convey the intended mood.

To evaluate the frame-selection stage, we compute—for every frame in the exploration video—the cosine similarity between its visual embedding and the text embedding of

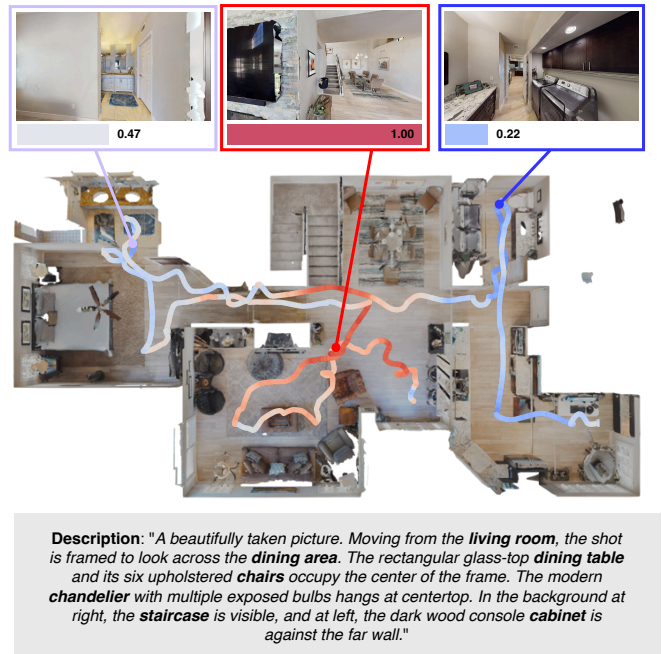


Fig. 5. The user-provided exploration video and instruction are first processed by a large language model into n waypoint descriptions. These descriptions are then converted into embeddings by a vision foundation model. Finally, the large language model selects n waypoint trios.

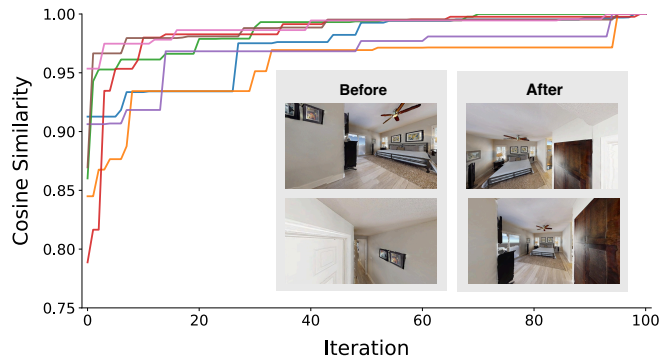


Fig. 6. **Pose-refinement robustness.** Cosine similarity between the current view and the reference view at \mathbf{T}^* over 100 iterations for seven random initializations within 1 m. All trials rapidly converge toward 1.0, indicating reliable alignment to the target viewpoint. Thumbnails show the view before refinement (“Before”) and after refinement (“After”).

the selected waypoint description (Sec. III-A). We project frame locations onto the floor plan and visualize the per-location scores as a heatmap (Fig. 5). Warm regions align with the intended area (e.g., the dining room), and the insets show the highest-scoring frames. These results indicate that retrieval (frame selection) reliably localizes the region of interest and provides strong initializations for subsequent pose refinement.

C. Pose Refinement Robustness Studies

To evaluate the robustness of our pose-refinement method, we find a waypoint $\mathbf{T}^* \in \text{SE}(3)$ and randomly sample seven

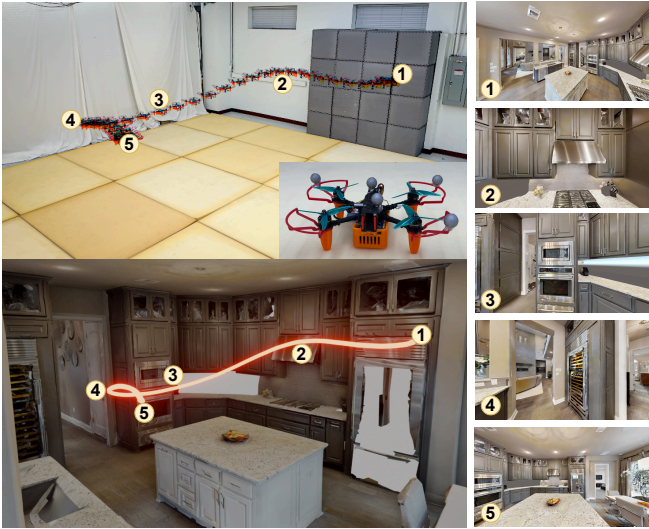


Fig. 7. **Hardware-in-the-loop experiment.** *Bottom-left:* the orange path shows experimental drone trajectory visualized in a reconstructed kitchen. *Right:* first-person views associated with each waypoint. *Top-left:* the experimental trajectory flaw by a real quadrotor. *Inset:* the quadrotor used.

initial poses $\{\mathbf{T}_0^{(k)}\}_{k=1}^7$ within 1 m of \mathbf{T}^* . Using the large language model generated description \mathcal{D}^* at \mathbf{T}^* , we run refinement for each of $\{\mathbf{T}_0^{(k)}\}_{k=1}^7$ for 100 iterations. At each iteration, we render image I_t given pose \mathbf{T} , and acquire image embedding of current refinement pose each iteration I_t as $\mathbf{i}_t = \phi_{\text{img}}(I_t)$. We also embed \mathbf{T}^* with ϕ_{img} to get embedding \mathbf{i}_t^* and record the cosine similarity between \mathbf{i}_t^* and \mathbf{i}_t at each iteration. As shown in Fig. 6, all seven runs converges to a cosine similarity of ~ 1 within 100 iterations. Notably, the randomized initializations—including arbitrary yaw—thus create cases where the target object is initially out of view, yet still converge within our standard 100-iteration.

D. Hardware in the Loop Validation

To verify that our simulated quadrotor dynamics faithfully reflect reality, we conducted hardware-in-the-loop (HIL) tests on the platform shown in Fig. 7. The vehicle carries an NVIDIA Jetson Orin NX running the autopilot stack. External pose estimates from a motion-capture system are fused with onboard IMU measurements to produce full 6-DoF odometry. The quadrotor platform is able to complete the flight within centimeter-level difference to simulation.

E. User Studies

We evaluated prompt–video alignment with a preference-based study: 41 participants rated, on a 1–5 scale (higher is better), how well each of the six outputs in Fig. 4 matches its prompt. We report mean in Fig 8. The ordering of scenes and videos follows their left-to-right layout in Fig. 4.

Rather than benchmarking against a single expert trajectory, we adopt preference-based evaluation because open-ended prompts admit multiple valid flights. Even expert-designed paths can differ substantially in trajectory distance

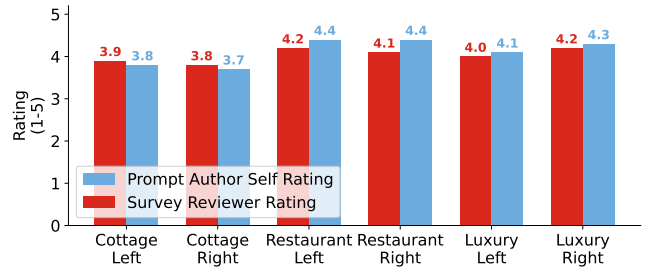


Fig. 8. **User study ratings.** Mean 1–5 Likert scores (higher is better) for prompt–video alignment across six outputs: *Cottage* (Left/Right), *Restaurant* (Left/Right), and *Luxury* (Left/Right), ordered as in Fig. 4. Bars show independent participant ratings from 41 users (author of prompt self-ratings shown for reference), indicating medium-high prompt–video alignment across different scenes.

while both satisfy intent and aesthetic criteria, making point-wise and path-wise distances to a fixed reference largely uninformative. By contrast, preference ratings directly measure the construct of interest—prompt–video alignment and perceived cinematographic quality—without relying on arbitrary geometric surrogates.

V. CONCLUSION

We introduced ACDC, a language-conditioned autonomous cinematography system that bridges abstract human intent and executable UAV trajectories. By combining semantic retrieval, preference-based optimization, and safe, dynamically feasible trajectory generation, ACDC enables non-experts to produce professional-grade indoor drone videos from natural-language prompts. Experiments in photorealistic simulation, hardware-in-the-loop testing, and user studies show that ACDC is robust to prompt abstraction, generalizes across diverse indoor scenes, and executes reliably on physical hardware. For future work, we aim to demonstrate an end-to-end, fully on-board system that performs 3D reconstruction from exploratory video, real-time localization and collision avoidance to capture cinematic video in the real world.

ACKNOWLEDGMENT

The authors thank Wenda Zhao for experimental support and H S Helson Go for his contribution in the development of the autopilot stack.

REFERENCES

- [1] T. Nägeli, J. Alonso-Mora, A. Domahidi, D. Rus, and O. Hilliges, “Real-time motion planning for aerial videography with dynamic obstacle avoidance and viewpoint optimization,” *IEEE Trans. Robot. Automat.*, vol. 2, no. 3, pp. 1696–1703, 2017.
- [2] R. Bonatti, W. Wang, C. Ho, A. Ahuja, M. Gschwindt, E. Camci, E. Kayacan, S. Choudhury, and S. Scherer, “Autonomous aerial cinematography in unstructured environments with learned artistic decision-making,” *Journal of Field Robotics*, vol. 37, no. 4, pp. 606–641, 2020.
- [3] P. Pueyo, J. Dendarieta, E. Montijano, A. C. Murillo, and M. Schwager, “Cinempc: A fully autonomous drone cinematography system incorporating zoom, focus, pose, and scene composition,” *IEEE Transactions on Robotics*, vol. 40, pp. 1740–1757, 2024.

- [4] M. Ahn, A. Brohan, *et al.*, “Do as i can, not as i say: Grounding language in robotic affordances,” *arXiv*, 2022.
- [5] D. Driess, F. Xia, M. S. M. Sajjadi, C. Lynch, A. Chowdhery, B. Ichter, A. Wahid, J. Tompson, Q. Vuong, T. Yu, W. Huang, Y. Chebotar, P. Sermanet, D. Duckworth, S. Levine, V. Vanhoucke, K. Hausman, M. Toussaint, K. Greff, A. Zeng, I. Mordatch, and P. Florence, “Palme: An embodied multimodal language model,” in *Proceedings of the 40th International Conference on Machine Learning (ICML)*, ser. Proceedings of Machine Learning Research, vol. 202. PMLR, 2023, pp. 8469–8488.
- [6] D. Shah, B. Osinski, B. Ichter, and S. Levine, “Lm-nav: Robotic navigation with large pre-trained models of language, vision, and action,” in *Proceedings of The 6th Conference on Robot Learning (CoRL)*, ser. Proceedings of Machine Learning Research, vol. 205. PMLR, 2023, pp. 2642–2654.
- [7] J. Xiao, C. W. Tsao, Y. Zhang, and M. Feroskhan, “Fm-planner: Foundation model guided path planning for autonomous drone navigation,” *arXiv preprint arXiv:2505.20783*, 2025.
- [8] G. Aikins, M. P. Dao, K. J. Moukpe, T. C. Eskridge, and K. Nguyen, “Leviosa: Natural language-based uncrewed aerial vehicle trajectory generation,” *Electronics*, vol. 13, no. 22, p. 4508, 2024.
- [9] H. Liang, J. Li, T. Bai, X. Huang, L. Sun, Z. Wang, C. He, B. Cui, C. Chen, and W. Zhang, “Keyvideollm: Towards large-scale video keyframe selection,” *arXiv*, 2024.
- [10] S. Zhang *et al.*, “Q-Frame: Query-aware frame selection and multi-resolution adaptation for video-llms,” *arXiv preprint arXiv:2506.22139*, 2025.
- [11] J. González, Z. Dai, A. Damianou, and N. D. Lawrence, “Preferential Bayesian optimization,” in *Proceedings of the 34th International Conference on Machine Learning*, ser. Proceedings of Machine Learning Research, vol. 70. PMLR, 2017, pp. 1282–1291.
- [12] W. Chu and Z. Ghahramani, “Preference learning with gaussian processes,” in *Proceedings of the 22nd International Conference on Machine Learning (ICML ’05)*. ACM, 2005, pp. 137–144.
- [13] R. A. Bradley and M. E. Terry, “Rank analysis of incomplete block designs: I. the method of paired comparisons,” *Biometrika*, vol. 39, no. 3-4, pp. 324–345, 1952.
- [14] Q. Galvane, J. Fleureau, F. Tariolle, and P. Guillotel, “Automated cinematography with unmanned aerial vehicles,” in *Proceedings of the Eurographics Workshop on Intelligent Cinematography and Editing (WICED)*. Eurographics Association, 2016.
- [15] B. Jeon and H. J. Kim, “Integrated motion planner for real-time aerial videography with a drone in a dense environment,” in *2020 IEEE International Conference on Robotics and Automation (ICRA)*. IEEE, 2020, pp. 1243–1249.
- [16] T. Nägeli, L. Meier, A. Domahidi, J. Alonso-Mora, and O. Hilliges, “Real-time planning for automated multi-view drone cinematography,” *ACM Trans. Graph.*, vol. 36, no. 4, July 2017.
- [17] C. Huang, F. Gao, J. Pan, Z. Yang, W. Qiu, P. Chen, X. Yang, S. Shen, and K. T. Cheng, “ACT: An autonomous drone cinematography system for action scenes,” in *2018 IEEE International Conference on Robotics and Automation (ICRA)*. IEEE, 2018, pp. 7039–7046.
- [18] M. Gschwindt, E. Camci, R. Bonatti, W. Wang, E. Kayacan, and S. Scherer, “Can a robot become a movie director? learning artistic principles for aerial cinematography,” in *Proceedings of the IEEE/RSJ International Conference on Intelligent Robots and Systems (IROS)*. IEEE, November 2019, pp. 1107–1114.
- [19] O. Limoyo, J. Li, D. Rivkin, J. Kelly, and G. Dudek, “PhotoBot: Reference-guided interactive photography via natural language,” in *2024 IEEE/RSJ International Conference on Intelligent Robots and Systems (IROS)*. IEEE, 2024, pp. 2479–2486, preprint: arXiv:2401.11061.
- [20] X. Liu, Y.-W. Tai, and C.-K. Tang, “ChatCam: Empowering camera control through conversational ai,” in *Advances in Neural Information Processing Systems (NeurIPS) 2024 Poster Track*, 2024, poster; Project page and preprint available.
- [21] Z. Xu, L. Wang, J. Wang, Z. Li, S. Shi, X. Yang, Y. Wang, B. Hu, J. Yu, and M. Zhang, “FilmAgent: A multi-agent framework for end-to-end film automation in virtual 3d spaces,” in *Technical Communications of SIGGRAPH Asia 2024*. ACM, 2024, pp. 1–4.
- [22] A. Jiao, T. P. Patel, S. Khurana, A. Korol, L. Brunke, V. K. Adajania, U. Culha, S. Zhou, and A. P. Schoellig, “Swarm-GPT: Combining large language models with safe motion planning for robot choreography design,” in *NeurIPS 2023 Workshop on Robot Learning: Pretraining, Fine-Tuning, and Generalization with Large Scale Models*, New Orleans, USA, 2023, workshop paper.
- [23] A. Radford, J. W. Kim, C. Hallacy, A. Ramesh, G. Goh, S. Agarwal, G. Sastry, A. Askell, P. Mishkin, J. Clark, G. Krueger, and I. Sutskever, “CLIP: Learning transferable visual models from natural language supervision,” in *International Conference on Machine Learning (ICML)*, 2021, arXiv preprint arXiv:2103.00020.
- [24] S. Patel, N. Keetha, A. Khandelwal, L. Weihs, R. Wang, and A. Kembhavi, “AM-RADIO: Agglomerative multimodal retrieval for efficient and domain-invariant object understanding,” *arXiv preprint arXiv:2312.06709*, 2023.
- [25] X. Zhai, B. Mustafa, L. Beyer, A. Kolesnikov, J. Puigcerver, A. Steiner, and N. Houlsby, “SigLIP 2: Multimodal pretraining with improved representations and zero-shot transfer,” *arXiv preprint arXiv:2502.14786*, 2025.
- [26] H. Liang, J. Li, T. Bai, X. Huang, L. Sun, Z. Wang, C. He, B. Cui, C. Chen, and W. Zhang, “KeyVideoLLM: Towards large-scale video keyframe selection,” *CoRR*, vol. abs/2407.03104, 2024, iCLR 2025 Spotlight acceptance.
- [27] N. V. Keetha, A. Mishra, J. Karhade, K. M. Jatavallabhula, S. Scherer, and M. Krishna, “AnyLoc: Towards universal visual place recognition,” *IEEE Robotics and Automation Letters (RA-L)*, vol. 8, no. 9, pp. 5561–5568, 2023.
- [28] K. Garg, S. S. Puligilla, S. Kolathaya, M. Krishna, and S. Garg, “Revisit Anything: Visual place recognition via image segment retrieval,” in *Computer Vision – ECCV 2024*. Springer, 2024, pp. 326–343.
- [29] A. Khandelwal, L. Weihs, R. Mottaghi, and A. Kembhavi, “Simple but Effective: Clip embeddings for embodied ai,” in *IEEE/CVF Conference on Computer Vision and Pattern Recognition (CVPR)*. IEEE, 2022, pp. 11 315–11 324.
- [30] D. S. Chaplot, R. Salakhutdinov, and A. Gupta, “Visual language maps for robot navigation,” in *Advances in Neural Information Processing Systems (NeurIPS)*, 2022.
- [31] E. Brochu, T. Brochu, and N. de Freitas, “A bayesian interactive optimization approach to procedural animation design,” in *Eurographics/ACM SIGGRAPH Symposium on Computer Animation (SCA)*, 2010, pp. 103–112.
- [32] Z. Li, Y. Liao, and C. Holz, “Efficient visual appearance optimization by learning from prior preferences,” in *Proceedings of the 38th Annual ACM Symposium on User Interface Software and Technology*, ser. UIST ’25. Busan, Republic of Korea: ACM, 2025.
- [33] U. Singhal, R. Feng, S. X. Yu, and A. Prakash, “Test-time canonicalization by foundation models for robust perception,” *arXiv preprint arXiv:2507.10375*, 2025.
- [34] J. Jung, Y. Jang, and J. S. Chung, “Test-time augmentation for pose-invariant face recognition,” *arXiv preprint arXiv:2505.09256*, 2025.
- [35] S. Majumder, T. Nagarajan, Z. Al-Halah, R. Pradhan, and K. Grauman, “Which viewpoint shows it best? language for weakly supervising view selection in multi-view instructional videos,” *arXiv preprint arXiv:2411.08753*, 2024, accepted to CVPR 2025 (Highlight).
- [36] C. Qin, M. S. Michet, J. Chen, and H. H.-T. Liu, “Time-optimal gate-traversing planner for autonomous drone racing,” in *2024 IEEE International Conference on Robotics and Automation (ICRA)*, 2024, pp. 8693–8699.
- [37] G. Comanici, E. Bieber, *et al.*, “Gemini 2.5: Pushing the frontier with advanced reasoning, multimodality, long context, and next generation agentic capabilities,” *arXiv preprint arXiv:2507.06261*, 2025.
- [38] M. Ranzinger, G. Heinrich, J. Kautz, and P. Molchanov, “Am-radio: Agglomerative vision foundation model reduce all domains into one,” in *Proceedings of the IEEE/CVF Conference on Computer Vision and Pattern Recognition (CVPR)*, June 2024, pp. 12 490–12 500.
- [39] M. Tschannen, A. Gritsenko, X. Wang, M. F. Naeem, I. Alabdulmohsin, N. Parthasarathy, T. Evans, L. Beyer, Y. Xia, B. Mustafa, O. Hénaff, J. Harmsen, A. Steiner, and X. Zhai, “Siglip 2: Multilingual vision-language encoders with improved semantic understanding, localization, and dense features,” *arXiv preprint arXiv:2502.14786*, 2025.
- [40] S. K. Ramakrishnan, A. Gokaslan, E. Wijmans, O. Maksymets, A. Clegg, J. M. Turner, E. Undersander, W. Galuba, A. Westbury, A. X. Chang, M. Savva, Y. Zhao, and D. Batra, “Habitat-matterport 3d dataset (HM3d): 1000 large-scale 3d environments for embodied AI,” in *Thirty-fifth Conference on Neural Information Processing Systems Datasets and Benchmarks Track*, 2021.